THE JOURNAL OF PHYSICAL CHEMISTRY B

ARTICLE

pubs.acs.org/JPCB

Aqueous Imidazole Solutions: A Structural Perspective from Simulations with High-Rank Electrostatic Multipole Moments

Steven Y. Liem,[†] Majeed S. Shaik,[†] and Paul L. A. Popelier*[,†,‡]

[†]Manchester Interdisciplinary Biocentre, University of Manchester, 131 Princess Street, Manchester M1 7DN, Great Britain

[‡]School of Chemistry, University of Manchester, Oxford Road, Manchester M13 9PL, Great Britain

ABSTRACT: Imidazole is a small but important molecule occurring as a structure fragment in systems from amino acids, over ionic liquids, to synthetic polymers. Here we focus on the structure and dynamics of imidazole in water at ambient conditions, using both radial and spatial distribution functions. Molecular dynamics simulations were carried out for various imidazole concentrations, using a traditional point-charge potential and a high-rank multipolar potential. The difference in the description of the electrostatics leads to sizable quantitative differences (e.g., the diffusion coefficient) but also qualitative differences in the local structure. In contrast to a point-charge potential, the multipolar potential favors hydrogen-bonded chainlike imidazole dimers over stacked dimers.

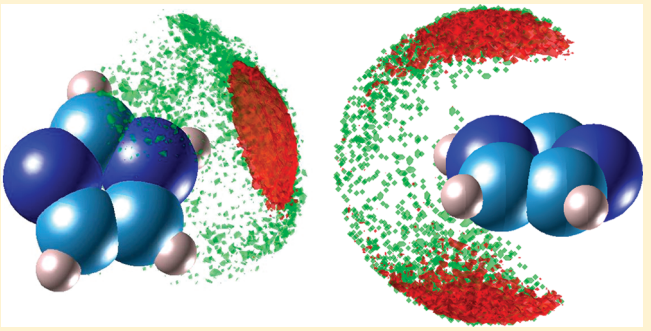

1. INTRODUCTION

Molecular self-assembly is a ubiquitous phenomenon occurring in naturally occurring molecular aggregates. The formation of molecular crystals is an example of such self-assembly process. Self-assembly processes can be described as a spontaneous organization of disordered molecules into ordered structures by noncovalent interactions. This concept has emerged as an attractive and rapidly growing technique in molecular engineering and has found a significant place in the fields of nanotechnology,[1,2] chemical synthesis,[3,4] polymer science,[5] materials, and engineering.[6] Intermolecular interactions such as $\pi-\pi$ interactions and weak hydrogen bonds play a key role in self-assembly. These interactions are the basis for the behavior of biological molecules such as nucleic acids, nucleotides, and enzymes. The knowledge of the self-assembly process involved in the simplest building blocks that constitute these biological molecules is especially important. In the current study we look at the behavior of one such important yet simple molecule in aqueous solution and study the behavior of imidazole in aqueous solution at different concentrations. Note that the term concentration always refers to a solution of imidazole (solute) in water (solvent).

Imidazole is important in both biology and chemistry. This five-membered aromatic heterocyclic compound is present in histidine, hemoglobin,[7] and other biomolecules and has significant medicinal properties[8] (e.g., antifungal agents, radiosensitizer). Imidazole is also used in the synthesis of ionic liquids, which are recognized as environment-friendly solvents or green solvents.[9] The water solubility of imidazole derivatives makes them applicable for biological purposes. From very early imidazole studies[10] it was established that the imidazole molecules self-assembled in nonpolar solvents, but the experimental techniques failed to show such mechanism in aqueous solution. However, in the UV study by Peral and Gallego,[11] it was suggested that imidazole and its methyl derivatives show self-association in aqueous solutions, even at very low concentrations. They proposed a model of *stacked* imidazole rings in aqueous solution to account for the hypochromic deviations observed. In their energy-dispersive X-ray diffraction study of concentrated imidazole water solutions (4.5 and 7.6 M), Gontrani et al.[12] noticed similar behavior. A set of five stacked imidazole molecules, varied in terms of center-of-mass distances and relative orientations, resulted in the best least-squares refinement. This arrangement corresponded to a "pseudohelix" in which stacked dimers interact with each other in a progression of short−long−short−long distances. It is surprising that neither study proposes the existence of chainlike or T-shaped imidazole assemblies. The latter were observed by McDonald and Jorgensen[13] in their pure liquid imidazole Monte Carlo simulations using the OPLS-AA force field[14] and were also reported by molecular dynamics (MD) simulations on pure liquid imidazole[15] carried out an electrostatic potential derived from quantum chemical topology (QCT).[16,17] Microhydrated environments of imidazole were also studied[18] in the context of imidazole's ionization. Understanding the influence of the solvent water is very important for the interpretation of (subfemtosecond) photoelectron spectroscopic measurements, which have recently become possible with the advent of liquid microjets.

Received: June 7, 2011
Revised: August 24, 2011
Published: August 26, 2011

dx.doi.org/10.1021/jp2053234 | *J. Phys. Chem. B* 2011, 115, 11389–11398

In this work we are interested in the influence of the electrostatic part of an interaction potential on the structure of aqueous imidazole solutions at different concentrations. In particular, we contrast the predictions made by a high-rank multipolar potential with a classical atomic charge model with one point charge per nucleus, namely, that of AMBER. As we will see the predictions are *qualitatively* different, which reinforces the need to work with electrostatics beyond the traditional paradigm of point charges, as embodied in the AMBER force field. Much attention has been devoted to understanding the convergence behavior of QCT multipolar expansion of the interatomic Coulomb and electrostatic interaction.[19−25] The finite nature of the topological atoms enables exact formal convergence, which cannot be attained by the distributed multipole analysis (DMA) moments,[26] because this method samples electron density over whole space rather than a finite volume. The QCT multipolar electrostatic potential has been used in MD simulations of liquid hydrogen fluoride,[27] liquid water,[28−30] and liquid imidazole.[15] In this work we focus on aqueous imidazole solutions, of varying and rather high concentration (∼0.5−8 M). The simulations carried out here complement those on pure liquid imidazole and are again done without including polarization.

It is useful to see the current work in the wider context of a coherent research program that we are carrying out. One may wonder if polarization, which is lacking in the current study, may be added at some later stage. The answer is yes and in a consistent and direct manner, avoiding long-range Rayleigh−Schrödinger perturbation theory. We have shown before that machine learning can model polarization in the framework of a QCT multipolar potential, for both intramolecular polarization[31] as well as intermolecular polarization.[32,33] However, this method has not yet been fully implemented and tested in a simulation package. This major modification will replace an earlier avenue of QCT and polarizability[34] explored in the context of long-range Rayleigh−Schrödinger perturbation theory. This machine-learning QCT approach, which is in progress, also offers an alternative to conformationally dependent DMA moments.[35]

2. BACKGROUND AND METHOD

2.1. The QCT Interatomic Potential. In this study, atomic multipole moments are defined from electron density fragments called atomic basins. The latter naturally arise by tracing the gradient paths in the electron density.[16] The gradient of a quantum mechanical three-dimensional (3D) scalar field of interest is the only concept needed to partition a system into (topological) subspaces. This is the basis of a method rooted in quantum mechanics[36] called QCT, a name introduced some time ago[24] and recently justified again in the introduction of ref 37. Multipole moments are formulated in the spherical tensor formalism[38] in order to avoid redundant components. This means, for example, that the hexadecupole moment of a topological (or QCT) atom has only 9 components instead of the 81 components that the Cartesian formalism would introduce.

The total potential energy $E_p(\Omega_A, \Omega_B)$ between any two (topological) atoms A and B consists of two contributions:

$$E_p(\Omega_A, \Omega_B) = E_{elec}(\Omega_A, \Omega_B) + 4\varepsilon_{AB}\left[\left(\frac{\sigma_{AB}}{R_{AB}}\right)^{12} - \left(\frac{\sigma_{AB}}{R_{AB}}\right)^{6}\right] \quad (1)$$

The first term corresponds to the electrostatic interaction energy $E_{elec}(\Omega_A, \Omega_B)$, whereas the second term embodies the Lennard-Jones (LJ) potential, which takes care of repulsion and dispersion, and R_{AB} is the distance between the nuclei of atoms Ω_A and Ω_B. The LJ interaction contains the parameters ε_{AB} and σ_{AB}, which correspond to the well depth and collision diameter, respectively. The electrostatic term is evaluated by means of a multipole expansion:

$$E_{elec}(\Omega_A, \Omega_B) = \sum_{l_A l_B m_A m_B} Q_{l_A m_A} T_{l_A m_A l_B m_B} Q_{l_B m_B} \quad (2)$$

where $T_{l_A m_A l_B m_B}$ is the interaction tensor, which is a purely geometric expression depending on R_{AB} and the orientation of the local axis system of atom Ω_A relative to that of atom Ω_B. The quantities Q_{lm} are the $2l + 1$ multipole moments of rank l with respect to the local axis system of either atom Ω_A or Ω_B. They are obtained by integrating the total charge density times the appropriate regular normalized spherical harmonic over the volume of a topological atom. The energy expression of eq 1 describes more accurately the short-range electrostatic interaction than the traditional point-charge expression. The latter is in fact the first term of the series expansion shown in eq 1, that is, when $l_A = l_B = m_A = m_B = 0$, and T_{0000} is simply $1/R_{AB}$. A detailed description on how $E_{elec}(\Omega_A, \Omega_B)$ is calculated can be found in a previous article.[19] The rank L conveniently describes to which extent two atoms Ω_A and Ω_B interact electrostatically. This rank is defined as $L = l_A + l_B + 1$. The higher the value of rank L the more features of the electron density are taken into account. When $L = 1$, the most elementary (i.e., least accurate) interaction occurs between two monopole moments (i.e., point charges). Only when the two monopole sites, that is, the nuclei, are sufficiently far apart will the interaction energy become exact. The monopole moments of topological atoms are not designed to accurately reproduce the electrostatic potential they generate. In QCT, a monopole moment is what it is: the most elementary summary of an atom's electron density. It is obtained directly from the electron density. Its value is compatible with a chemist's intuition on electronegativity. It is the higher rank multipole moments, starting with the dipole moment, that systematically refine the description of an atom's electron density, until a sufficiently accurate (and possibly exact, convergence allowing) reproduction of the electrostatic potential is obtained. In an MD study on liquid water,[28] we have shown before, using the oxygen−oxygen radial distribution function (RDF) at 1 atm and 300 K, that $L = 5$ is essential to recover the typical features of a liquidlike structure, such as the mandatory appearance of a second peak, right of the first and major peak. In the simulations of this work L is also set to 5, which means that quadrupole−quadrupole, dipole−octupole, and monopole−hexadecupole interactions are included. Finally, it is useful to mention here that analytical first and second derivatives of the energy in eq 1 with respect to nuclear displacement have been available for some time.[39] These analytical forces and Hessian enable a robust exploration of potential energy surfaces.[40,41]

For the current study, we have adopted the same set of multipole moments and LJ parameters that we used in the examination of pure liquid imidazole[15] and liquid water.[30] Table 1 lists the values for these parameters, and its concomitant diagram introduces an intuitive atomic labeling scheme. For example, N_H is the nitrogen atom in the five-membered heterocycle to which a hydrogen is bonded, whereas =C(N_H) is the atom in the C=C double bond, bonded to N_H. Note that all hydrogen atoms,

Table 1. Lennard-Jones Parameters for the Different Atom Types in Imidazole and Water

Atom	ε (kJmol^{-1})	σ (Å)
O	0.7861	3.135
H_w	0.015	0.663
N_H	0.7113	3.25
$C(N_H)$	0.36	3.4
C(N)	0.36	3.4
$(N)C(N_H)$	0.36	3.4
N	0.7113	3.25
$H(N_H)$	0.066	1.07
$H(=C(N_H))$	0.063	2.51
H(=C(N))	0.063	2.51
$H(N)C(N_H)$	0.063	2.42

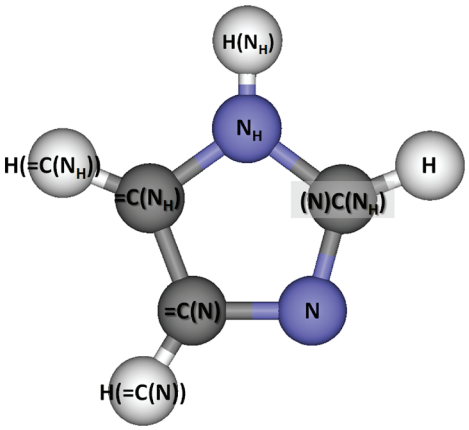

including that of water, have nonvanishing values for σ. The geometries of monomeric water and monomeric imidazole were optimized using GAUSSIAN03[42] at the CCSD/aug-cc-pVTZ[43] level of theory. Multipole moments for all atoms in imidazole and water were computed from the corresponding wave functions using the program MORPHY98[44−46] with default parameters. For the LJ interactions, the Lorentz−Berthelot mixing rules[47] were used when evaluating interactions between different atom types.

2.2. Details of the Multipolar Simulations and the Point-Charge Simulations. First we discuss the details of the multipolar simulations. These simulations were performed with the program DLMULTI,[48] which is derived from the popular program DLPOLY.[49] A major feature of DLMULTI is the implementation of a multipolar Ewald summation scheme to account for the long-range nature of the multipolar interactions. Note that this scheme has been implemented for high-rank multipolar interactions, up to $L = 5$. All simulations were carried out using an isothermal−isobaric ensemble using the Berendsen thermostat[50] and barostat.[51] We have conducted a series of room-temperature simulations of imidazole solutions at different imidazole concentrations. The first[28] of our previous studies on liquid water showed that a system containing 216 molecules is sufficient to replicate several properties of liquid water such as the RDF and the self-diffusion coefficient. In this work, the same number of water molecules is used with different numbers of imidazole molecules (2−32) to perform simulations at the designated concentrations (see Table 2). All simulations were carried out at room temperature and pressure (i.e., 298 K and 1 atm) using the NPT ensemble. For every concentration, the system was allowed to equilibrate for at least 100 ps prior to production runs of 1 ns with a time step of 0.5 fs to integrate the equations of motion.

Second, we provide details on the point-charge simulations. In order to contrast the effects of the QCT potential with a traditional point-charge-based force field, we performed simulations at similar concentrations but using a system that is roughly 8 times larger than the QCT system. The all-atom AMBER ff99SB force field[52] was used in conjunction with the AMBER simulation package.[53] MD simulations were carried out using periodic boundary conditions and a near cubic rectangular simulation cell. Electrostatic interactions were calculated with the particle-mesh Ewald method.[54] We used a cutoff of 8 Å for the real-space direct sum part of the Ewald summation and for the van der Waals interactions. The Berendsen coupling algorithm[50] was applied, and the two-staged equilibration procedure used in our recent study of liquid imidazole[15] was also adopted to equilibrate the system prior to the production run of 2 ns. Similarly to the QCT system, simulations were carried out using the NPT ensemble at 298 K and 1 atm. The equations of motion were integrated with a time step of 0.5 fs.

Finally we note that both imidazole and water were treated as rigid bodies in the QCT simulations but as flexible molecule in the AMBER simulations. In our previous simulations[15] on pure liquid imidazole we showed that the imidazole ring deformations are fairly small, as well as the out-of-plane bending motions of the C and H atoms. Hence, we believe that it is safe enough to compare the results from the (flexible) point-charge model with those of the (rigid body) multipolar model.

Table 2. Concentrations of Simulated Solutions and the Number of Imidazole and Water Molecules in the Simulation Systems

	no. of imidazole molecules	
imidazole concn (M)	QCT[a]	AMBER[b]
8.22	32	256 (1728)
7.71	30	240 (1727)
7.19	28	224 (1730)
6.68	26	208 (1724)
6.17	24	192 (1728)
5.65	22	176 (1724)
5.14	20	160 (1730)
4.62	18	144 (1733)
4.11	16	128 (1730)
3.60	14	112 (1724)
3.08	12	96 (1732)
2.57	10	80 (1730)
2.06	8	64 (1728)
1.54	6	48 (1731)
1.03	4	32 (1726)
0.51	2	16 (1724)

[a] The number of water molecules is always 216 for QCT simulations. [b] The number in parentheses is the number of water molecules.

dx.doi.org/10.1021/jp2053234 |J. Phys. Chem. B 2011, 115, 11389–11398

Table 3. Measured Density of Imidazole Solutions at Different Imidazole Concentrations

concn (M)	density (g cm^{-3})
0.03	0.999
0.06	0.998
0.13	0.999
0.26	0.999
0.51	1.000
1.03	1.001
2.06	1.005
4.11	1.014
6.94	1.030
8.22	1.057

2.3. Density Determination. Because the densities of the various imidazole solutions at different concentrations are not available from the literature, we measured them ourselves in order to compare with the densities generated from our simulations. The densities were determined by measuring the mass of each solution, contained in a 25 mL flask. A predetermined amount of imidazole corresponding to the required concentration was dissolved in distilled water to make up a 50 mL solution. Part of this solution was then transferred to a 25 mL glass flask with a stopper. The glass flask was weighed to an accuracy of four significant figures, before and after the solution was added. This procedure was carried out for all the concentrations. The density of each imidazole solution is given in Table 3. These densities will be referred to as the experimental values in this study. We believe that our measured densities are reliable enough for the purpose of this study because they are in line with the more accurate experimental measurements that we have identified. For example, the density of pure water at 25 °C is 0.9970479 g cm^{-3} and the density of pure imidazole at 101 °C is 1.0303 g cm^{-3}.

2.4. Analysis of Local Structure. The local structure of the water and imidazole molecules in each solution was examined by means of RDFs, three-dimensional spatial distribution functions (SDFs), and geometrical criteria distinguishing stacked and chain imidazole dimer arrangements, discussed in section 2.5. The RDFs were obtained for the following $\Omega_A\cdots\Omega_B$ interactions, where Ω_A and Ω_B are atoms of interest: (N)C(N_H)···O, =C(N_H)···O, =C(N)···O, N_H···N, and N_H···N_H. An SDF is a useful tool to gain detailed insight in the local environment adjacent to an atom of interest. In this work, SDFs were obtained for N_H···N_H, N···O, N_H···O, and (N)C(N_H)···O interactions at an imidazole concentration of 5.65 M. In the above $\Omega_A\cdots\Omega_B$ notation, we adhere to the convention, valid for both RDF and SDF, that atom Ω_A belongs to the central molecule, whereas atom Ω_B represents a neighboring atom. Note that for RDF the program AMBER allows this neighboring atom to be in the same molecule that houses the central atom. The detailed procedure followed to generate the SDFs has been explained before, in our work on liquid imidazole.[15]

2.5. Dimer Assembly Analysis. For an aqueous imidazole solution, the ability of imidazole molecules to self-associate and form π-stacked or chainlike assemblies has been studied experimentally.[11,12] Our simulations enable the study of this behavior and the assessment of the influence of the potential. However, RDFs and SDFs are rather limited in their ability to provide useful information in this regard. A more direct approach

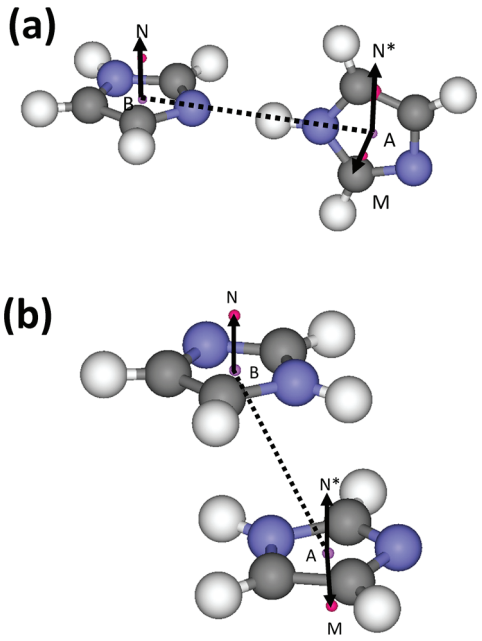

Figure 1. Optimized geometries of the imidazole dimer in the gas phase: (a) chain dimer, (b) stacked dimer. The small spheres, A and B, represent the centroids of the two molecules, whereas the small spheres, M and N, are surface normals (where N* represents the surface normal translated from B to A).

is examining the self-association behavior through the geometric characteristics of imidazole dimers identified from the snapshots of a simulation. On the basis of the geometries of gas-phase imidazole dimers optimized using GAUSSIAN03,[42] we defined a set of geometric parameters that can be used to classify the dimer assemblies (see Figure 1). For *chain* assemblies, the five geometric parameters are (1) the distance between the donor (N_H) and acceptor atom N, (2) the distance d(A, B) between the centroids A and B in Figure 1 (each is defined as the geometric center (or barycenter) of the aromatic ring consisting of the non-hydrogen atoms only), (3) the hydrogen bond angle ∠N_HH-(N_H)N (i.e., the angle formed by three atoms involved in the hydrogen bond N_H−H(N_H)···N), (4) the angle (∠MAN*, Figure 1) between the surface normals (which is the normal to the plane of the aromatic ring), and finally (5) the angle (∠MAB, Figure 1) between the line linking the centroids and the surface normal of the neighboring molecule. Because *stacked* assemblies cannot form hydrogen bonds only parameters 2, 4, and 5 are meaningful, that is, d(A, B), ∠MAN*, and ∠MAB. Table 4 lists all five geometric parameters, with the values we propose for them in order to decide if a dimer is in a chain or a stacked arrangement. Table 4 lists as the "mean value" (i.e., expected value), as well as the range, which marks the maximum deviation allowed. For example, if the d(A, B) distance of a pair of dimers is between 3.29 and 3.69 Å then the dimers obey one of the criteria for stacking. There are three such geometric criteria for stacked dimers and five for chain dimers. The criteria given in Table 4 are rather strict, defining unambiguous chainlike or stackedlike arrangements. As a result there are arrangements that are neither stacked or in a chain configuration.

In order to examine the effect of concentration as well as the nature of the electrostatic interaction (i.e., multipole moment or point charge) on the system, it is essential to determine the

Table 4. Geometric Criteria for the Classification of Chain and Stacked Imidazole Dimer Assemblies[a]

	chain		stacked	
geometric parameter	mean value	range	mean value	range
(1) distance (Å) between atoms N_H and N	2.85 Å	0.20 Å	N/A	N/A
(2) distance d(A, B) (Å) between the centroids A and B	5.14 Å	0.86 Å[b]	3.49 Å	0.2
(3) hydrogen-bond angle ∠N_HH(N_H)N (deg)	175°	20°	N/A	N/A
(4) angle (∠MAN*) (deg) between surface normals	91°	10°	175°	10°
(5) angle (∠MAB) (deg) between a surface normal and the vector joining the centroids A and B	94°	30°	151°	10°

[a] Table 1 and Figure 1 clarify the symbols used. [b] The only relevant boundary is the upper boundary of 6 Å (= 5.14 + 0.86 Å).

number of different dimer assemblies in the system. For this purpose we defined a quantity called *normalized occurrence*, which characterizes the number of stacked or chain assemblies in the system. To calculate its value for a particular type of assembly occurring in a simulation, a number of snapshots of the system, $N_{snapshots}$, are stored during this simulation. For each snapshot *all* possible pairs of imidazole molecules are examined. In each snapshot a Kronecker δ function decides if a pair is stacked or chainlike by checking if the pair obeys, respectively, the three or five geometric criteria discussed above. More precisely, if we look for a stacked dimer in a snapshot k the Kronecker $\delta_k(i,j)$ returns 1 if all criteria are obeyed, where i and j each represent an imidazole molecule in a given imidazole pair. Otherwise, the Kronecker δ function returns a zero. The treatment is similar if we look for a chainlike dimer. When all the snapshots have been examined, the final value is normalized by $N_{snapshots}$ and by the number of imidazole molecules in the system, denoted N_{Im}, or

$$\text{normalized occurrence} = \frac{1}{N_{snapshots}N_{Im}} \sum_{k}^{N_{snapshots}} \sum_{i}^{N_{Im}} \sum_{j>i}^{N_{Im}} \delta_k(i,j) \quad (3)$$

3. RESULTS AND DISCUSSION

3.1. Analysis of System Density and Self-Diffusion Coefficient. Figure 2 compares the equilibrated system densities of both the QCT and AMBER simulations to the experimental values. It shows that, independent of the force field used, the density of the solution increases with concentration. For the QCT potential, it is clear that the density of the solution is very close to the values of the experimental concentrations up to approximately 5 M beyond which the density starts to deviate gradually more from experiment. The difference at the highest concentration is about 1%. However, the QCT results do seem to possess the same type of curvature that is just detectable in the experimental profile. For the AMBER force field, the simulated densities are consistently lower than experiment, by about 1.5%. Nevertheless, we believe the agreement can be improved upon with additional tuning of the AMBER force field. In addition, in contrast to the trend observed for the QCT force field, the quadratic interpolation curve of AMBER's densities suggests a nearly linear increase with the solution concentration. The favorable behavior of the QCT densities may be seen as encouraging because the only tunable parameters in the QCT potential are the LJ parameters. Having said this, the experimental measurements of the densities have not been carried out that accurately, such as with a modern densitometer.

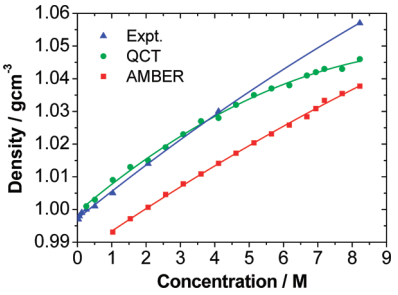

Figure 2. Comparison of the system density at various simulated imidazole concentrations. The curves are least-squares fits using a second-order polynomial.

Table 5. List of Selected Atomic Self-Diffusion Coefficients Obtained for AMBER and QCT Simulations

	self-diffusion coefficient/$\times 10^{-9}$ m^2 s^{-1}			
	AMBER		QCT	
IM concn (M)	N_H	O	N_H	O
8.22	1.43	3.32	0.40	1.26
7.71	1.77	3.30	0.39	1.30
7.19	1.47	3.44	0.67	1.23
6.68	1.78	3.57	0.50	1.24
6.19	1.97	3.49	0.74	1.32
5.65	1.85	3.92	0.46	1.32
5.14	1.89	3.99	0.64	1.33
0.51	3.51	5.28	0.28	1.91

In addition to the system density, we examined the self-diffusion coefficients D of the ring atom N_H, and of the oxygen atom of a water molecule (see Table 5). Due to the small number of imidazole molecules in the QCT system, the values for N_H have large uncertainties but can still offer some insight in the overall behavior of diffusion at different concentrations. For both AMBER and QCT, the general trend is one of a reduction in the value of D with increasing concentration, indicating that the solution becomes more viscous. At the lowest concentration, the self-diffusion coefficient of oxygen indeed approaches an oft-quoted experimental value[55] of pure liquid water, which is 2.30 $\times$ 10^{-9} m^2 s^{-1}. We also note that the self-diffusion coefficients predicted by AMBER are significantly higher than those predicted by the QCT force field. A possible explanation is the use of

dx.doi.org/10.1021/jp2053234 |J. Phys. Chem. B 2011, 115, 11389–11398

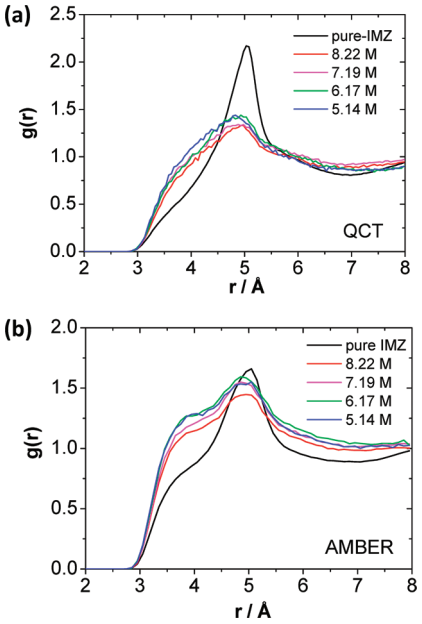

Figure 3. Comparison of $N_H \cdots N_H$ RDFs for (a) QCT and (b) AMBER simulations at selected imidazole concentrations.

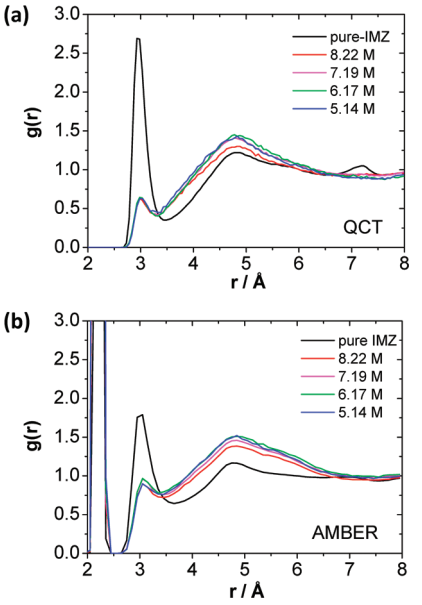

Figure 4. Comparison of $N_H \cdots N$ RDFs for (a) QCT and (b) AMBER simulations at selected imidazole concentrations.

the TIP3P potential for the water molecule in the AMBER system, which is known[56] to overestimate D of pure liquid water (i.e., 5.2×10^{-9} m^2 s^{-1}). To the best of our knowledge no experimental value for the self-diffusion coefficient of imidazole (in aqueous solution or pure) has been reported so far. Nevertheless, on the basis of the success of QCT, as opposed to AMBER, in predicting the asymptotic value of D for pure water, we are reasonably confident that the QCT values of D for imidazole in water can be trusted as well. This assertion is made against the background of corresponding AMBER values of D that are about 3 times as large as those of QCT.

3.2. Local Structure Analysis. Here we are interested in the effect a potential has on the local environment of individual atoms. The RDFs for $N_H \cdots N_H$ at five selected concentrations are presented in Figure 3. For both AMBER and QCT, the features of the RDF seem to undergo a smooth transition from low imidazole concentration in water to pure liquid imidazole. Apart from the pure liquid, we observed a broad peak with similar heights at a distance of about 5 Å for both potentials. This peak most likely corresponds to the distance between N_H and N_H in hydrogen-bonded imidazole dimers because in this type of dimer this distance frequently occurs, whereas in the stacked dimer it is too far from the expected value of around 3.1 Å, as determined from the gas-phase optimized stack dimer. Note that this distance is not part of the criteria in Table 4 because it is already covered by the centroid criterion in that table. In the AMBER simulations, a strong shoulder appears on the left of the main peak, in the interval of 3.5−4.5 Å. The QCT potential has a similar trait in the same distance range but not as pronounced. This shoulder disappeared almost completely in the QCT simulation of the pure liquid imidazole system that we reported on before.[15] However, in the AMBER simulations, the shoulder can still be seen for pure liquid imidazole. We believe that the shoulder marks the existence of imidazole dimers with a stacking arrangement, stabilized by $\pi-\pi$ interaction, or the existence of other non-hydrogen-bonded dimer configurations.

Figure 4 shows the $N_H \cdots N$ RDFs for (a) QCT and (b) AMBER, which can be directly compared because they are on the same scale. Each $g(r)$ profile shows a smooth transition from low to high imidazole concentration. Admittedly, there is a gap between the profile of the highest (solute) concentration of 8.22 M and the profile of pure liquid imidazole, which corresponds to 16 M. We believe that this increase in peak height for pure imidazole liquid is caused by the fact that there is no competition from water molecules to form hydrogen bonds to the N atoms (see later discussion on SDF). For the solutions, the large amount of water present in the system means that it is more likely for an imidazole molecule to form hydrogen bonds with adjacent water molecules. Hence, there is a lower first peak in Figure 4 for both systems. The location of the first (intermolecular) peak (on the left, at 3 Å) and the second peak (between 4.5 and 5.0 Å) is comparable for both potentials. The additional AMBER peak at the utmost left (∼2.3 Å) corresponds to the intramolecular $N_H \cdots N$ distance, which is excluded in QCT simulations because they are purely intermolecular. For pure liquid imidazole, the height of the first intermolecular QCT peak (3 Å) of about 2.7 is significantly higher than the AMBER peak height of about 1.8. The area under the QCT peak is much larger than that under the AMBER peak, demonstrating that QCT predicts chains to be more prevalent in pure liquid imidazole. We can conclude this because the distance of this peak is consistent with the distance between the N and N_H atoms of a hydrogen-bonded imidazole dimer. The much lower peak heights for the aqueous solutions compared to pure liquid imidazole are probably due to oxygens of water molecules competing with N of imidazole to form hydrogen bonds with N_H. For the QCT system, the peak heights for the four plotted concentrations are almost identical, at about 0.6. For the AMBER simulations, the values are always higher and in the range from 0.8 to 1.0. This seems to suggest that AMBER predicts a slight preference of hydrogen-bonded dimer chains compared to QCT. We should emphasize that a RDF is *not* a precise tool to deduce hydrogen bonding. This is why we will look again at the local

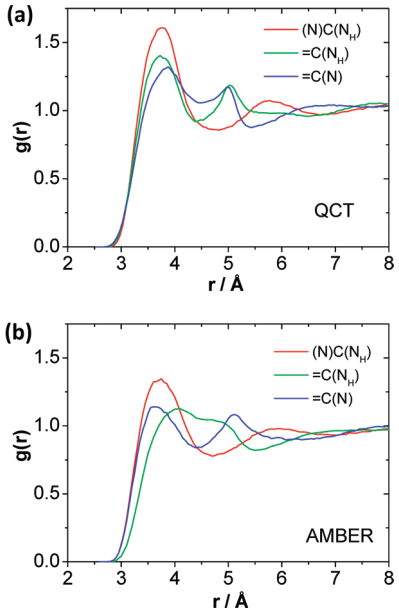

Figure 5. Comparison of C···O RDFs for (a) QCT and (b) AMBER simulations at 6.17 M (imidazole).

structure by means of SDFs and a "normalized occurrence" function defined above, which classifies dimer configurations according to the geometric criteria of Table 4. The height of the second peak, both in AMBER and QCT in Figure 4, cannot resolve the matter because it is virtually the same between both potentials, at about 1.2.

Figure 5 shows C···O RDFs, where C (central atom) is one of the three possible carbon atoms in the imidazole ring and O is an oxygen atom in a neighboring water. Here we contrast the local environments from the perspective of the carbon atoms. The RDFs for the QCT simulation are given in Figure 5a, which shows that the first peaks (left) for all three carbons practically coincide, in the region of 3.7−3.8 Å. However, one expects the carbon atoms $=C(N_H)$ and $=C(N)$ to show similar RDF profiles because both atoms are bonded to a single nitrogen atom, whereas the $(N)C(N_H)$ carbon atom is bonded to two nitrogens. The first peak is indeed more pronounced for $(N)C(N_H)$. More profound differences between $(N)C(N_H)$ on one hand, and $=C(N_H)$ and $=C(N)$ on the other, appear when looking at the second peaks. Whereas the second peaks of $=C(N_H)$ (green) and $=C(N)$ (blue) are equally high and both located at 5.0 Å, there is a trough here for the $(N)C(N_H)$ (red) profile. This carbon's second peak is situated much further out, at 5.7 Å. The RDFs of the AMBER simulations in Figure 5b share these broad features with the QCT RDFs. The area under the $(N)C(N_H)$ (red) QCT profile is larger than that under the AMBER profile, implying that QCT predicts a higher coordination of oxygen atoms around $(N)C(N_H)$. In order to interpret this on firmer grounds SDFs need to be inspected, as will be done below in Figure 6d.

The overall features of the $=C(N)$ and $(N)C(N_H)$ profiles are comparable but with minor differences in terms of peak height and depth of the valley between the first two peaks. The most striking difference is the near merging of the first and second peak of $=C(N_H)$ (green) into a first peak and a shoulder. The precise physical interpretation of these observations is difficult to make apart from stating that the first peak in the RDFs corresponds to

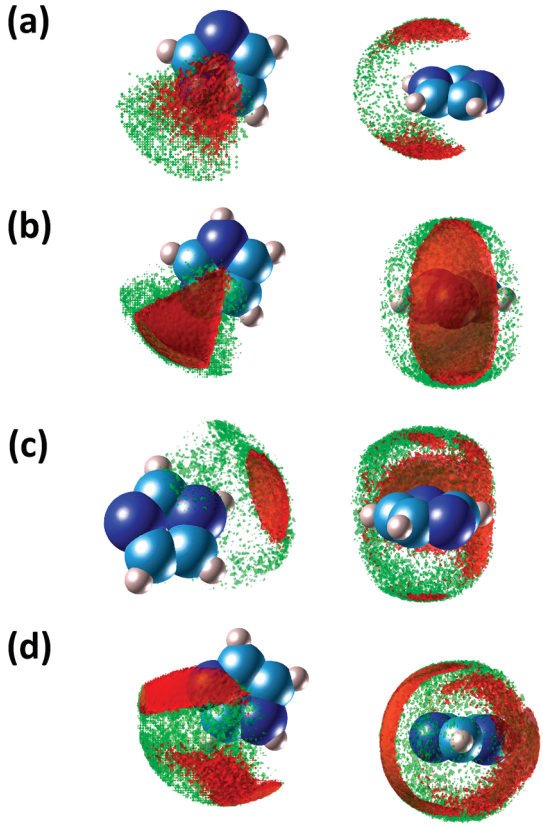

Figure 6. Comparison of QCT (green) and AMBER (red) in terms of spatial distribution functions of (a) $N_H\cdots N_H$ [isovalue = 3.0 for both top (left) and front view (right)], (b) $N\cdots O$, isovalue = 2.0, (c) $N_H\cdots O$ [isovalue = 3.0 for front view (left) and 2.0 (right)], and (d) $(N)C(N_H)\cdots O$, isovalue = 2.0. The carbon atoms are shaded in light blue.

the (intermolecular) C···O distance. In summary, the QCT and the AMBER potential do produce different local environments, both qualitatively different for $=C(N_H)$ only.

The local environments of different atoms were also examined by means of SDFs. They provide a more detailed picture of the distribution of a particular type of neighboring atom surrounding a central atom. Figure 6a shows the effects of the QCT and AMBER potentials on the SDF for $N_H\cdots N_H$. The first notable difference is that the AMBER distribution (red) of N_H atoms adjacent to the central N_H is predominantly located in two distinctive triangular regions centered almost directly above and below the central N_H atom, and roughly parallel to the molecular plane of the central molecule. *This suggests the strong presence of imidazole dimers with a stacked conformation*. The occurrence of neighboring N_H atoms in the space between the triangular regions is low and seems to decrease rapidly (to almost zero) when approaching the space directly opposite to the N−H bond axis. The situation is different for the QCT potential. Here the distribution (green) in Figure 6a is more homogeneous and crescentlike, indicating the presence of both stacked and hydrogen-bonded dimers around the central molecule.

Figure 6b examines the distribution of water molecules around the N atom. Here the distributions from the QCT and AMBER simulations are similar with only minor differences. For both types of simulation, the distribution resembles a crescent with its tips lying directly above and below the center of the aromatic

dx.doi.org/10.1021/jp2053234 |J. Phys. Chem. B 2011, 115, 11389–11398

ring. The difference between the two systems is marked by the homogeneity and the width of the distribution. For the AMBER potential (red) the distribution is represented by a well-defined homogeneous and solid crescent. In contrast, the QCT distribution (green) has a wider crescent, with edges populated increasingly thinning from the top and bottom toward the level of the imidazole ring.

Figure 6c shows the distribution of water molecules around the central N_H atom. This $N_H\cdots O$ SDF shows that the distribution of oxygen atoms adjacent to N_H (AMBER, red) is asymmetrical at lower isovalues, such as 2.0. At the higher isovalue of 3.0, the distribution becomes more circular and its center coincides with the N−H bond axis (which is hidden from view). In contrast, the distribution of neighboring oxygen atoms in the QCT simulations (green) is always symmetrical and centered on the N−H bond axis. In addition, at the higher isovalue, the distribution becomes a central circular disk with an outer concentric ring.

The results from Figure 4 and Figure 6, parts b and c, point to the fact that, for both systems, the water molecule competes with imidazole molecules to form hydrogen bonds with imidazole molecules. For each system, the larger number of water molecules in the solution means it is more likely for an imidazole molecule to form a hydrogen bond with water rather than with another imidazole molecule. Consequently, the height of the first peak in Figure 4 is expected to be lower than that of the pure imidazole liquid.

Finally, Figure 6d demonstrates the difference between AMBER and QCT from the point of view of how the acidic carbon sees the surrounding water molecules, via the $(N)C(N_H)\cdots O$ SDF. On the right of the right panel AMBER shows a crescent shape, which does not extend to above and below the imidazole ring. QCT shows a symmetrical and spread out (i.e., diffuse) SDF, whereas the AMBER SDF shows two blobs.

It is tempting to link the observations made above with low-energy gas-phase minima of imidazole−water complexes, $Im\cdots(H_2O)_n$, where n can vary between 1 and 5. Previous work[18] reported such minima computed at MP2/aug-cc-pVDZ level. For n = 1, the lowest energy minimum (binding energy 31 kJ mol^{-1}) involves a water hydrogen-bonded to N. This strong minimum is recovered in the red crescent (AMBER) showing up as a triangle in Figure 6b (left), which corresponds to the presence of $N\cdots H(-O)$ hydrogen-bonded dimers. There is a substantial patch of green (QCT) overlapping with the red crescent, confirming that QCT also recovers the $N\cdots H(-O)$ hydrogen bond in this n = 1 minimum. In fact, all $Im\cdots(H_2O)_n$ clusters with $n \geq 2$ contain a water hydrogen-bonded to this N atom. There are four low-energy minima for the $Im\cdots(H_2O)_4$ clusters, three of them having almost the same geometry. Here, all waters approximately lie in the imidazole plane and form a ring of waters hydrogen-bonded to each other. The ring is attached to N at one end and N_H at the other end, again through $N\cdots H(-O)$ and $N_H\cdots O$ hydrogen bonds, respectively. The geometry of the fourth minimum is very different from the other three, because now the water ring is oriented almost perpendicularly to the imidazole ring. This type of configuration may explain the presence of SDF density above the imidazole plane, for both potentials, appearing in Figure 6, parts b and c.

Features in the $N_H\cdots O$ SDF of Figure 6c can be linked to the second lowest minimum (26 kJ mol^{-1}) in $Im\cdots(H_2O)$. This strong minimum is recovered in the red blob (AMBER) at the back of the SDF of Figure 6c (left), which corresponds to the presence of $N_H\cdots O$ hydrogen-bonded dimers. Although barely visible in this figure, full inspection of the 3D SDF confirms a circular green blob (QCT) overlapping with the red one. Finally, we link observations in Figure 6d with the $Im\cdots(H_2O)_2$ complex. For the QCT system, there is some evidence pointing at $(N)C(N_H)\cdots O$ dimers in the system, because Figure 6d shows a sizable green zone in the region between N and $(N)C(N_H)$. This green zone is not mirrored by a red zone in the AMBER system. In $Im\cdots(H_2O)_2$, the low-energy minimum has a water, which forms a hydrogen bond to the (rather acidic) $(N)C(N_H)$, resulting in a $C-H\cdots O$ hydrogen bond. This water molecule is in the above-mentioned green zone of the QCT system.

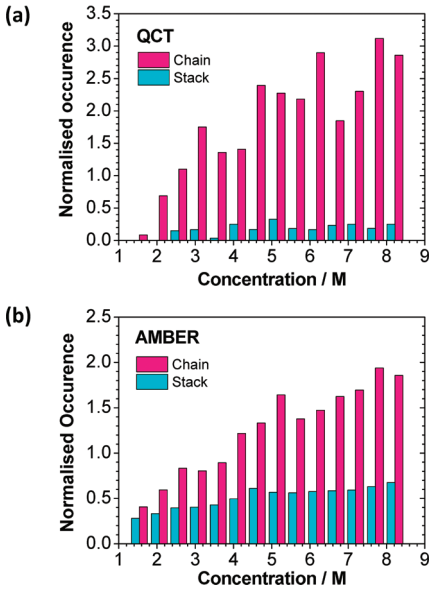

Figure 7. Distribution of stacked and chain dimers vs imidazole concentration for (a) QCT simulations and (b) AMBER simulations.

3.3. Self-Assembly of Imidazole Molecules. The phenomenon of imidazole molecules self-assembling and forming dimer conformations was studied previously by experiment. The procedure of the "normalized occurrence", as described in section 2.5, leads to Figure 7. We would like to point out again that the results for the QCT system at lower concentrations (e.g., <5 M) are subjected to large uncertainties. Nevertheless, we consider the overall picture to be useful and provide a qualitative picture of imidazole assembly.

The most significant observation deduced from Figure 7 is that the QCT (Figure 7a) and AMBER (Figure 7b) potential generate systems with different dimer distribution characteristics. Nevertheless, both potentials confirm the simultaneous presence of chainlike and stacked dimers in the system. Our findings agree with previous experimental studies[11,12] of aqueous imidazole solutions where the existence of stacked dimers was suggested. However, Figure 7 shows that the number of chainlike and stacked dimers in the system, as well as their ratio, are different between the two potentials. *First, the number of chainlike dimers in the QCT system is consistently higher than in the AMBER system,* around 1.5 times at higher concentrations. In addition, whereas the AMBER profiles tend to be more linearly increasing with concentration, for both chains and stacks, the QCT profiles show more asymptotic character. *Second, the number of stacked dimers in the QCT system is at best half the number in the AMBER system, for*

each concentration. This trend is thus opposite to that observed for chainlike dimers. The conclusion that stacked dimers dominate in the AMBER system agrees with the AMBER RDF profiles of $N_H\cdots N_H$ (Figure 3b) where more pronounced shoulders appear between 3.5 and 4.0 Å, which we also attributed to the existence of stacked or stackedlike dimers. It also agrees with the conclusion reached from the $N_H\cdots N_H$ SDF in Figure 6a. A third way of interpreting the data in Figure 7 is taking the ratio of the number of chain dimers over the number of stacked dimers, once for QCT and again separately for AMBER. This ratio clearly favors chainlike dimers in QCT.

An important comment concerns the actual appearance of imidazole in water, which is relevant with an eye on future contact with modern experiment. In the current work, imidazole was represented with two inequivalent nitrogen atoms, that is, one N bonded to a H, and one N not. However, it is known that, in aqueous solution, the proton bonded to one N in imidazole can migrate to the other N. Compared to a single MD time step (0.5 fs), this proton interconversion is relatively slow (~10 ps or 20 000 time steps). Which experimental technique, then, is fast enough to perceive imidazole in the way that the current MD simulations perceive it, i.e., with only one N being protonated at any one time? It is not NMR spectroscopy because (at high pH) this technique detects only one single ^{15}N line, corresponding to two equivalent nitrogens. Because of NMR's time resolution of 10^{-5} s it fails to see the rapid N−H proton exchange between the two nitrogen atoms of neutral imidazole in water. Again, this chemical−structural interconversion occurs on the 10^{-11} s (or 10 ps) time scale. Nevertheless, NMR chemical shifts are good indicators of hydrogen-bond interactions.[57] A technique that does perceive two inequivalent nitrogens is photoelectron spectroscopy. It has a time resolution of 10^{-17} s (or 0.01 fs), which is so fast that it can see a single MD snapshot. This technique can detect distinct binding-energy peaks in both nitrogen 1s and carbon 1s photoelectron spectra.[58] This type of spectroscopy in aqueous solution is still a young field with few publications but with enormous potential.

A second comment on contact with experiment concerns very recent work[59] on complexes of imidazole and water (and imidazole and methanol), using supersonic jet FTIR spectroscopy (supplemented by ^{18}O substitution). These experiments unambiguously show that water prefers to act as an O−H···N hydrogen-bond donor toward imidazole, instead of acting as a N−H···O acceptor.

In this study, we employed the TIP3P potential as a point-charge model to describe the water molecule. We believe that the diffusion coefficient of both water and imidazole in the system has been overestimated by TIP3P. However, we envisage that even for a point-charge water potential yielding a more realistic diffusion coefficient (e.g., SPC/E), some differences in the local environment of an imidazole molecule will still be detected. It would be interesting to conduct a more systematic study to compare and contrast other point-charge water potentials with our QCT model.

4. CONCLUSION

For the first time an electrostatic potential based on high-rank atomic multipole moments (computed according to QCT) has been used to study aqueous imidazole solutions by MD simulations. We contrasted the results of this QCT potential (without polarization) to those of a classical point-charged-based potential (AMBER). Simulations at room temperature and pressure were performed for aqueous imidazole solutions at different concentrations from 0.5 M (not shown in Figure 7) to 8.2 M. The density of the solutions in QCT simulations depended on concentration, in very good agreement with experiment up to 5 M, after which QCT started underestimating experiment. The AMBER potential consistently underestimated the solution's density for all concentrations by almost 0.02 g cm^{-3}. The predicted diffusion coefficient decreased with increasing concentration for both potentials. The QCT system recovered the diffusion coefficient for pure water (in the limit of infinite dilution). In contrast, AMBER predicts a significantly overestimated diffusion coefficient for pure water.

The local structure around imidazole was investigated via RDFs and SDFs. The two potentials resulted in notably different local environments. AMBER's pronounced shoulder in the $N_H\cdots N_H$ RDF suggests stacked dimers. The only marked difference in the C···O RDFs is in the profile of $=C(N_H)\cdots O$. The differences in the SDFs are more prominent. The most important difference lies in the presence of chain versus stacked dimer assemblies in the simulated system. In agreement with previous experimental studies, both potentials confirm the presence of stacked dimers. However, the number of each type of dimer and the ratio between the types are significantly different among the two potentials. For chains, the number for the QCT potential is considerably higher than for the AMBER potential. For stacks, the amount in the AMBER system can be almost double that of the QCT system. The ratio of stacked dimers over chain dimers is much lower for the QCT potential.

AUTHOR INFORMATION

Corresponding Author

*E-mail: pla@manchester.ac.uk.

REFERENCES

(1) Whitesides, G. M.; Mathias, J. P.; Seto, C. T. *Science* **1991**, *254*, 1312–1319.
(2) Huie, J. C. *Smart Mater. Struct.* **2003**, *12*, 264–271.
(3) Lawrence, D. S.; Jiang, T.; Levett, M. *Chem. Rev.* **1995**, *95*, 2229–2260.
(4) Stoddart, J. F.; Tseng, H. R. *Proc. Natl. Acad. Sci. U.S.A.* **2002**, *99*, 4797–4800.
(5) Zhang, S. G.; Altman, M. *React. Funct. Polym.* **1999**, *41*, 91–102.
(6) Schnur, J. M. *Science* **1993**, *262*, 1669–1676.
(7) Ghosh, J. *A Textbook of Pharmaceutical Chemistry*; Chand & Company Limited: New Delhi, India.
(8) Edwards, P. *Drug Discovery Today* **2001**, *6*, 1072.
(9) Petkovic, M.; Seddon, K. R.; Rebelo, L. P. N.; Pereira, C. S. *Chem. Soc. Rev.* **2011**, *40*, 1383–1403.
(10) Hoffman, K. *Imidazole and Its Derivatives, Part 1*; Interscience: New York, 1953; Vol. 6.
(11) Peral, F.; Gallego, E. *J. Mol. Struct.* **1997**, *415*, 187–196.
(12) Gontrani, L.; Caminiti, R.; Bencivenni, L.; Sadun, C. *Chem. Phys. Lett.* **1999**, *301*, 131–137.
(13) McDonald, N. A.; Jorgensen, W. L. *J. Phys. Chem. B* **1998**, *102*, 8049–8059.
(14) Jorgensen, W. L.; Maxwell, D. S.; Tirado-Rives, J. *J. Am. Chem. Soc.* **1996**, *118*, 11225–11236.
(15) Shaik, M. S.; Liem, S. Y.; Yuan, Y.; Popelier, P. L. A. *Phys. Chem. Chem. Phys.* **2010**, *12*, 15040–15055.
(16) Bader, R. F. W. *Atoms in Molecules. A Quantum Theory*; Oxford University Press: Oxford, Great Britain, 1990.
(17) Popelier, P. L. A. Quantum Chemical Topology: on Bonds and Potentials. In *Structure and Bonding. Intermolecular Forces and Clusters*;

Wales, D. J., Ed.; Springer: Heidelberg, Germany, 2005; Vol. 115; pp 1−56.
(18) Jagoda-Cwiklik, B.; Slavicek, P.; Cwiklik, L.; Nolting, D.; Winter, B.; Jungwirth, P. *J. Phys. Chem. A* **2008**, *112*, 3499–3505.
(19) Popelier, P. L. A.; Joubert, L.; Kosov, D. S. *J. Phys. Chem. A* **2001**, *105*, 8254–8261.
(20) Popelier, P. L. A.; Kosov, D. S. *J. Chem. Phys.* **2001**, *114*, 6539–6547.
(21) Rafat, M.; Popelier, P. L. A. *J. Chem. Phys.* **2006**, *124*, 144102.
(22) Rafat, M.; Popelier, P. L. A. *J. Comput. Chem.* **2007**, *28*, 292–301.
(23) Rafat, M.; Popelier, P. L. A. *J. Chem. Phys.* **2005**, *123*, 204103–204101, 204107.
(24) Popelier, P. L. A.; Aicken, F. M. *Chem. Phys. Chem.* **2003**, *4*, 824–829.
(25) Solano, C. J. F.; Pendás, A. M.; Francisco, E.; Blanco, M. A.; Popelier, P. L. A. *J. Chem. Phys.* **2010**, *132*, 194110.
(26) Stone, A. J. *Chem. Phys. Lett.* **1981**, *83*, 233–239.
(27) Liem, S.; Popelier, P. L. A. *J. Chem. Phys.* **2003**, *119*, 4560–4566.
(28) Liem, S. Y.; Popelier, P. L. A.; Leslie, M. *Int. J. Quantum Chem.* **2004**, *99*, 685–694.
(29) Liem, S. Y.; Popelier, P. L. A. *J. Chem. Theory Comput.* **2008**, *4*, 353–365.
(30) Shaik, M. S.; Liem, S. Y.; Popelier, P. L. A. *J. Chem. Phys.* **2010**, *132*, 174504.
(31) Darley, M. G.; Handley, C. M.; Popelier, P. L. A. *J. Chem. Theory Comput.* **2008**, *4*, 1435–1448.
(32) Handley, C. M.; Popelier, P. L. A. *J. Chem. Theory Comput.* **2009**, *5*, 1474–1489.
(33) Handley, C. M.; Hawe, G. I.; Kell, D. B.; Popelier, P. L. A. *Phys. Chem. Chem. Phys.* **2009**, *11*, 6365–6376.
(34) in het Panhuis, M.; Popelier, P. L. A.; Munn, R. W.; Angyan, J. G. *J. Chem. Phys.* **2001**, *114*, 7951–7961.
(35) Koch, U.; Popelier, P. L. A.; Stone, A. J. *Chem. Phys. Lett.* **1995**, *228*, 253–260.
(36) Bader, R. F. W.; Popelier, P. L. A. *Int. J. Quantum Chem.* **1993**, *45*, 189–207.
(37) Popelier, P. L. A.; Bremond, E. A. G. *Int. J. Quantum Chem.* **2009**, *109*, 2542–2553.
(38) Stone, A. J. *The Theory of Intermolecular Forces*; Clarendon: Oxford, Great Britain, 1996.
(39) Popelier, P. L. A.; Stone, A. J. *Mol. Phys.* **1994**, *82*, 411–425.
(40) Popelier, P. L. A.; Stone, A. J.; Wales, D. J. *Faraday Discuss.* **1994**, *97*, 243–264.
(41) Joubert, L.; Popelier, P. L. A. *Phys. Chem. Chem. Phys.* **2002**, *4*, 4353–4359.
(42) Frisch, M. J.; Trucks, G. W.; Schlegel, H. B.; Scuseria, G. E.; Robb, M. A.; Cheeseman, J. R.; Montgomery, J. A., Jr.; Vreven, T.; Kudin, K. N.; Burant, J. C.; Millam, J. M.; Iyengar, S. S.; Tomasi, J. J.; Barone, V.; Mennucci, B.; Cossi, M.; Scalmani, G.; Rega, N.; Petersson, G. A.; Nakatsuji, H.; Hada, M.; Ehara, M.; Toyota, K.; Fukuda, R.; Hasegawa, J.; Ishida, M.; Nakajima, T.; Honda, Y.; Kitao, O.; Nakai, H.; Klene, M.; Li, X.; Knox, J. E.; Hratchian, H. P.; Cross, J. B.; Adamo, C.; Jaramillo, J.; Gomperts, R.; Stratmann, R. E.; Yazyev, O.; Austin, A. J.; Cammi, R.; Pomelli, C.; Ochterski, J. W.; Ayala, P. Y.; Morokuma, K.; Voth, A.; Salvador, P.; Dannenberg, J. J.; Zakrzewski, V. G.; Dapprich, S.; Daniels, A. D.; Strain, M. C.; Farkas, O.; Malick, D. K.; Rabuck, A. D.; Raghavachari, K.; Foresman, J. B.; Ortiz, J. V.; Cui, Q.; Baboul, A. G.; Clifford, S.; Cioslowski, J.; Stefanov, B. B.; Liu, G.; Liashenko, A.; Piskorz, P.; Komaromi, I.; Martin, R. L.; Fox, D. J.; Keith, T.; Al-Laham, M. A.; Peng, C. Y.; Nanayakkara, A.; Challacombe, M.; Gill, P. M. W.; Johnson, B.; Chen, W.; Wong, M. W.; Gonzalez, C.; Pople, J. A. *GAUSSIAN03*; Gaussian, Inc.: Pittsburgh, PA, 2003.
(43) Dunning, T. H. J. *J. Chem. Phys.* **1989**, *90*, 1007.
(44) Popelier, P. L. A. *Comput. Phys. Commun.* **1998**, *108*, 180–190.
(45) Popelier, P. L. A. *Mol. Phys.* **1996**, *87*, 1169–1187.
(46) Popelier, P. L. A. *Chem. Phys. Lett.* **1994**, *228*, 160–164.
(47) Allen, M. P.; Tildesley, D. J. *Computer Simulations of Liquids*; Oxford University Press: Oxford, Great Britain, 1993.
(48) Leslie, M. *Mol. Phys.* **2008**, *106*, 1567–1578.
(49) Smith, W.; Leslie, M.; Forester, T. R. *DLPOLY*; Council for the Central Laboratory of the Research Councils, Daresbury Lab: Daresbury, Warrington WA4 4AD, England, 2003.
(50) Berendsen, H. J. C.; Postma, J. P. M.; Van Gunsteren, W. F.; Dinola, A.; Haak, J. R. *J. Chem. Phys.* **1984**, *81*, 3684–3690.
(51) Berendsen, H. J. C.; Van Gunsteren, W. F. In *MD Simulations: Techniques and Approaches in Molecular Liquids, Dynamics and Interactions*; Barnes, A. J., Orville-Thomas, W. J., Yarwood, J., Eds.; Reidel: New York, 1984; pp 475−500.
(52) Hornak, V.; Abel, R.; Okur, A.; Strockbine, B.; Roitberg, A.; Simmerling, C. *Proteins: Struct., Funct., Bioinf.* **2006**, *65*, 712–725.
(53) Case, D. A.; Darden, T. A.; Cheatham, T. E., III; Simmerling, C. L.; Wang, J.; Duke, R. E.; Luo, R.; Merz, K. M.; Pearlman, D. A.; Crowley, M.; Walker, R. C.; Zhang, W.; Wang, B.; Hayik, S.; Roitberg, A.; Seabra, G.; Wong, K. F.; Paesani, F.; Wu, X.; Brozell, S.; Tsui, V.; Gohlke, H.; Yang, L.; Tan, C.; Mongan, J.; Hornak, V.; Cui, G.; Beroza, P.; Mathews, D. H.; Schafmeister, C.; Ross,W. S. ; Kollman, P. A. *AMBER 9*; University of California, San Francisco: San Francisco, CA, 2006
(54) Darden, T.; York, D.; Pedersen, L. *J. Chem. Phys.* **1993**, *98*, 10089–10092.
(55) Krynicki, K.; Green, C. D.; Sawyer, D. W. *Faraday Discuss.* **1978**, *66*, 199.
(56) Guillot, B. *J. Mol. Liq.* **2002**, *101*, 219–260.
(57) Wei, Y.; de Dios, A. C.; McDermott, A. E. *J. Am. Chem. Soc.* **1999**, *121*, 10389.
(58) Nolting, D.; Ottosson, N.; Faubel, M.; Hertel, I. V.; Winter, B. *J. Am. Chem. Soc.* **2008**, *130*, 8150–8151.
(59) Zischang, J.; Lee, J. J.; Suhm, M. A. *J. Chem. Phys.* **2011**, *135*, 061102, 1−3.